

See discussions, stats, and author profiles for this publication at: <https://www.researchgate.net/publication/273152338>

On the Properties of Ammonium Ion-Water Clusters: Analyses of Structure Evolution, Non-Covalent Interactions, and Temperature and Humidity Effects.

ARTICLE *in* THE JOURNAL OF PHYSICAL CHEMISTRY A · MARCH 2015

Impact Factor: 2.69 · DOI: 10.1021/jp512323k · Source: PubMed

READS

14

8 AUTHORS, INCLUDING:



Shuai Jiang

Chinese Academy of Sciences

16 PUBLICATIONS 35 CITATIONS

[SEE PROFILE](#)



Teng Huang

anhui Institute of Optics and Fine Mechanics,C...

32 PUBLICATIONS 146 CITATIONS

[SEE PROFILE](#)



Yu-Peng Zhu

University of Science and Technology of China

6 PUBLICATIONS 9 CITATIONS

[SEE PROFILE](#)



Wei Huang

Caterpillar Inc.

93 PUBLICATIONS 1,446 CITATIONS

[SEE PROFILE](#)

Properties of Ammonium Ion–Water Clusters: Analyses of Structure Evolution, Noncovalent Interactions, and Temperature and Humidity Effects

Shi-Tu Pei,[†] Shuai Jiang,[†] Yi-Rong Liu,[†] Teng Huang,[†] Kang-Ming Xu,[†] Hui Wen,[†] Yu-Peng Zhu,[†] and Wei Huang^{*,†,‡}

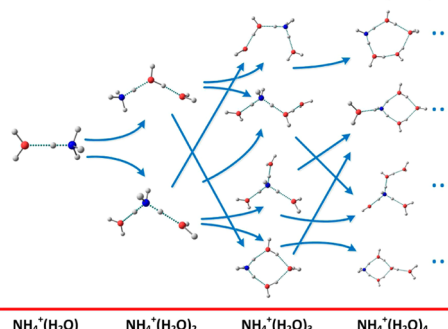
[†]Laboratory of Atmospheric Physico-Chemistry, Anhui Institute of Optics & Fine Mechanics, Chinese Academy of Sciences, Hefei, Anhui 230031, China

[‡]School of Environmental Science & Optoelectronic Technology, University of Science and Technology of China, Hefei, Anhui 230026, China

Supporting Information

ABSTRACT: Although ammonium ion–water clusters are abundant in the biosphere, some information regarding these clusters, such as their growth route, the influence of temperature and humidity, and the concentrations of various hydrated clusters, is lacking. In this study, theoretical calculations are performed on ammonium ion–water clusters. These theoretical calculations are focused on determining the following characteristics: (1) the pattern of cluster growth; (2) the percentages of clusters of the same size at different temperatures and humidities; (3) the distributions of different isomers for the same size clusters at different temperatures; (4) the relative strengths of the noncovalent interactions for clusters of different sizes. The results suggest that the dipole moment may be very significant for the ammonium ion–water system, and some new stable isomers were found. The nucleation of ammonium ions and water molecules is favorable at low temperatures; thus, the clusters observed at high altitudes might not be present at low altitudes. High humidity can contribute to the formation of large ammonium ion–water clusters, whereas the formation of small clusters may be favorable under low-humidity conditions. The potential energy surfaces (PES) of these different sized clusters are complicated and differ according to the distribution of isomers at different temperatures. Some similar structures are observed between $\text{NH}_4^+(\text{H}_2\text{O})_n$ and $\text{M}(\text{H}_2\text{O})_n$ (where M represents an alkali metal ion or water molecule); when $n = 8$, the clusters begin to form the closed-cage geometry. As the cluster size increases, these interactions become progressively weaker. The successive binding energy at the DF-MP2-F12/VDZ-F12 level is better than that at the PW91PW91/6-311++G(3df, 3pd) level and is consistent with the experimentally determined values.

Structural evolutions of the clusters $\text{NH}_4^+(\text{H}_2\text{O})_n$



I. INTRODUCTION

In the atmospheric sciences, aerosols are defined as a suspension of any particulate matter in a gas. Primary aerosols are released directly into the atmosphere from both natural and anthropogenic sources, such as the burning of biomass, combustion of fossil fuels, volcanic eruptions and wind-driven suspensions of soil, mineral dust, sea salt and biological materials. In contrast, secondary aerosols form in the atmosphere via different physical and chemical processes, and many of the physicochemical properties of substances are determined by hydrogen-bonding interactions.^{1,2} Aerosol particles affect the radiative balance by scattering and absorbing incoming radiation. Aerosols can significantly reduce visibility and also have potential health effects.^{3–6} The formation of new particles occurs in two stages,^{7,8} i.e., the nucleation stage to form a subcritical nucleus ($\sim 1\text{--}3$ nm in diameter), which is followed by the growth phase where the critical cluster increases in size.^{9,10} Nucleation is defined as the formation of

molecular seeds or clusters prior to the formation of a new phase. To understand the formation of aerosols, obtaining insights from the nucleation stage is of critical importance. However, experimentally obtaining such insights is difficult because the experimental sampling of aerosols is primarily limited to particles larger than 3 nm,^{11,12} which severely limits the availability of experimental data regarding small clusters. Furthermore, theoretical models are difficult simulate the formation of small clusters because they use bulk properties for describing aerosols.

Several atmospheric nucleation mechanisms have been proposed and relatively well studied, including the binary homogeneous nucleation of H_2SO_4 and H_2O ,^{13,14} the ternary homogeneous nucleation of H_2SO_4 , H_2O , and NH_3 ,^{15,16} ion-

Received: December 15, 2014

Revised: March 3, 2015

Published: March 3, 2015



induced nucleation,^{17–19} and organics-enhanced nucleation.^{20–22} However, the dominant mechanism in the atmosphere still remains unclear, primarily because the preferred mechanism for the formation of new particles is dependent on specific locations and times. The nucleation of ions is favored because small charged clusters have considerably higher thermodynamic stability.¹⁷ In addition, charged clusters grow faster than neutral clusters due to the dipole–charge interaction between charged clusters and strongly dipolar precursor molecules.¹⁹

Ammonium ions are produced in the atmosphere primarily from the agricultural release of ammonia,²³ which is converted to ammonium ions through reactions with water or other atmospheric species.²⁴ Ammonium plays a key role in the deposition of nitrogen and in controlling acidity in the environment,²⁵ and it forms potentially dangerous fine aerosol particles.²⁶ The ammonium ion is one of the most important ionic species in aqueous solutions, and ammonium ion–water clusters are abundant in the biosphere.²⁷ Thus, the ammonium ion is essential for modeling atmospheric processes. Some structures, electronic energies and free energies for $\text{NH}_4^+(\text{H}_2\text{O})_n$ ($n = 4–6$) have been experimentally determined;²⁸ however, these structures differ from the minimum energy structures determined through more recent *ab initio* calculations.^{29–32} Kim and co-workers conducted an extensive comparison of binding energies, enthalpies, and free energies determined using different functions.³⁰ $\text{NH}_4^+(\text{H}_2\text{O})_n$ ($n = 5–19$) clusters were investigated by Calvo's group.³¹ Zhao studied many conformations of $\text{NH}_4^+(\text{H}_2\text{O})_n$ ($n = 4–8$) clusters using the density functional theory-based tight-binding method.³² Morrell and Shields used the high-level MP2 calculation method with correlated basis sets to search the various conformations of $\text{NH}_4^+(\text{H}_2\text{O})_n$ ($n = 1–10$), and they determined the electronic and free energies at two different temperatures.³³

However, these studies primarily focused on the structures and energy levels of clusters. Knowledge of the growth path for clusters of ammonium ions and water molecules remains unclear, and the effects of temperature and humidity have not been investigated. Furthermore, the distribution of isomers of clusters has not been fully explored, and the strengths of the noncovalent interactions in $\text{NH}_4^+(\text{H}_2\text{O})_n$ clusters have not been investigated.

In this study, calculations at the DF-MP2-F12/VDZ-F12//PW91PW91/6-311++G(3df,3pd) level are performed to obtain the structures and energies for these clusters at 200–300 K and 1 atm. This work is a continuation of long-standing efforts to explore the pattern of $\text{NH}_4^+(\text{H}_2\text{O})_n$ cluster growth, the effects of temperature and humidity, noncovalent interactions of $\text{NH}_4^+(\text{H}_2\text{O})_n$ clusters, and the distribution of isomers at different temperatures. The results indicated that some similar structures exist between $\text{NH}_4^+(\text{H}_2\text{O})_n$ and $M(\text{H}_2\text{O})_n$ (where M represents a standard alkali metal ion or water molecule).

II. METHODS

We performed a basin-hopping (BH) global minimum search combined with a density functional theory (DFT) geometric optimization using DMol³ code³⁴ to obtain the low-lying structures of the $\text{NH}_4^+(\text{H}_2\text{O})_n$ ($n = 1–10$) cluster systems. The basin-hopping technique includes two procedures: First, a new structure is generated via the random displacement of molecules; then, the structure is optimized to the local minimum. Second, the local minimum is used as a criterion

to accept the initial generated structure spaces with Boltzmann weight at finite temperature. According to our calculation experiment, the hydrogen bond length changes from 1.8 Å, the rotation is set from 0 to $\pi/2$. The BH method used in our previous report.^{35,36} The top-five isomers of the $\text{NH}_4^+(\text{H}_2\text{O})_n$ ($n = 1–10$) systems were selected on the basis of their relative energies and were reoptimized using the PW91PW91 functional and the 6-311++(3df,3pd) basis set for all of elements in the Gaussian 09 software package.³⁷ Previous studies^{38–41} have indicated that PW91PW91/6-311++G(3df,3pd) provides better performance for predicting the vibrational spectrum of oxalic acid than MP2/6-311++G(3df,3pd) or B3LYP/6-311++(3df,3pd). Therefore, we employed the PW91PW91 functional to calculate the molecular geometries and energetics.

All of the clusters reported here are local minima on the potential energy surface, and there is no imaginary frequency for the optimized structures. All of the single-point energies of the low-energy structures at the PW91PW91 level were recalculated using the explicitly correlated second-order Møller–Plesset perturbation theory method with the density fitting (DF-MP2-F12) approximation and the VDZ-F12 basis set. The enthalpies [H(T)] and Gibbs free energies [G(T)] were calculated on the basis of the electronic energies obtained at the DF-MP2-F12/VDZ-F12 level. The contributions of the low-energy isomers were estimated using Boltzmann-averaged enthalpies and free energies. The standard conditions were a pressure of 1 atm and the stated temperature. We employed the reduced density gradient (RDG) approach that was recently proposed by Yang and co-workers implemented in Multiwfn 3.0,⁴² which has been confirmed to be effective and convenient for identifying noncovalent interactions.

III. RESULTS AND DISCUSSION

A. Geometries and Evolution of $\text{NH}_4^+(\text{H}_2\text{O})_n$ System.

The optimized geometries of $\text{NH}_4^+(\text{H}_2\text{O})_n$ ($n = 1–10$) at the PW91PW91/6-311++G(3df,3dp) level of theory are depicted in Figures 1–7, all of their structures and the single point energies can be obtained in Tables S2–S13 in the Supporting Information, and four possible evolution routes are presented in Figure 8.

When $n < 3$, as the number of water molecules increases, NH_4^+ tends to form the longest possible linear hydrogen bonds, but the geometry of $\text{NH}_4^+(\text{H}_2\text{O})_n$ tends to change from linear to circular. The clusters for $n \geq 3$ water molecules tend to form with a ring or symmetric cage geometry. The number of possible isomers of $\text{NH}_4^+(\text{H}_2\text{O})_n$ considerably increases as n (the number of water molecules) increases. For example, when $n = 1–2$, we only obtain one to three isomers; however, when n is greater than 3, we can obtain dozens of isomers of $\text{NH}_4^+(\text{H}_2\text{O})_n$. For ease of visualization, N atoms are shown in blue, and O and H atoms are shown in red and gray, respectively. The global minimum M_n geometry can generally be found from one of the low-lying isomers of M_{n-1} , where M represents the molecule in the formed clusters. Four evolution routes are shown in Figure 8.

For $\text{NH}_4^+(\text{H}_2\text{O})_n$ clusters, isomer 1a is observed to possess a linear chain geometry, and the length of the H bond between ammonium and water is 1.592 Å. Zhao and co-workers⁴³ observed an interesting isomer, which possessed a binary type of hydrogen bond geometry in which the oxygen atom of the water molecule and two hydrogen atoms of ammonium form two hydrogen bonds; however, this geometry was not observed in other works.^{44,45} To ensure that this geometry is a global

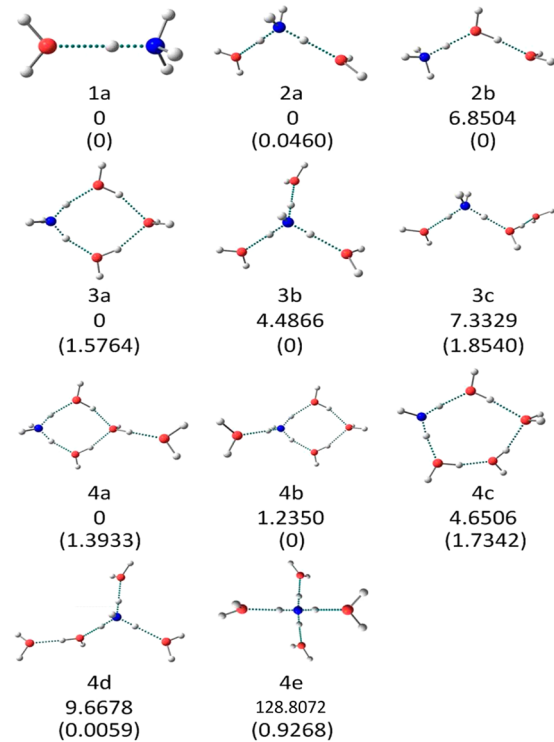


Figure 1. Optimized geometries of $\text{NH}_4^+(\text{H}_2\text{O})_n$ ($n = 1\text{--}4$). Relative energies are given in kcal/mol at the PW91PW91/6-311++G(3df,3pd) level, which are marked by na , nb , and nc , where the number n represents the cluster size; the energies at the DF-MP2-F12/VDZ-F12 level are presented in parentheses. For ease of visualization, N atoms are shown in blue, and O and H atoms are shown in red and gray, respectively.

minimum, we used a manual method to construct it, but further optimization resulted in the same geometry as 1a. For the case of $\text{NH}_4^+(\text{H}_2\text{O})_2$, the lengths of the H bonds in the 2a isomer are 1.682 and 1.673 Å. In this case, the ammonium ion and water molecule are arranged in a triangular geometry, and with the exception of the free hydrogen atoms and the two water molecules situated on the opposite side of the ammonium ion, this geometry is in agreement with previous studies.^{45,46} In our search for the global minimum of the $\text{NH}_4^+(\text{H}_2\text{O})_2$ cluster, we found another geometry, 2b, that is 0.046 kcal/mol lower in energy than 2a. Note that the 2b geometry was found in previous studies,⁴⁴ and it consists of two water molecules located on the same side of the ammonium ion. The 2a and 2b geometries may evolve from 1a.

The top-three low-lying geometries for $\text{NH}_4^+(\text{H}_2\text{O})_3$ are shown in Figure 1. Pickard et al. found that 3b is the lowest-energy geometry,⁴⁵ which appears as a tapered geometry. 3b is the lowest-energy isomer at the DF-MP2-F12/VDZ-F12 level, and in this isomer, the length of the H bond between ammonium and water is 1.742 Å. At the PW91PW91/6-311+G(3df,3pd) level, 3a is the lowest-energy isomer, and it is similar to the lowest-energy geometry of the pure water cluster of $(\text{H}_2\text{O})_4$ ^{47,48} and the lowest-energy geometry of $\text{K}^+(\text{H}_2\text{O})_3$,²⁹ thus, the ammonium hydrate may have some characteristics similar to those of pure water clusters and $\text{K}^+(\text{H}_2\text{O})_n$. The lowest-energy geometry of the $(\text{H}_2\text{O})_4$ cluster is a standard square; however, the lowest-energy geometry of the $\text{NH}_4^+(\text{H}_2\text{O})_3$ cluster is a distorted rhombus, in which the length of the H bond between ammonium and water is 1.656 Å

and the length of the H bond between water and water molecule is 1.902 Å. The C_3 isomer 3b is 0.0465 eV higher in energy than isomer 3a at the PW91PW91/6-311++G(3df,3pd) level. Compared with $\text{NH}_4^+(\text{H}_2\text{O})_n$ ($n = 1\text{--}2$), the $\text{NH}_4^+(\text{H}_2\text{O})_3$ monomer clearly undergoes a significant change in which the geometry changes from 2D to 3D. Configuration 3a may be produced from 2a or 2b, but 3b and 3c may evolve from 2a.

For the case of $\text{NH}_4^+(\text{H}_2\text{O})_4$, five lower-lying geometries for $\text{NH}_4^+(\text{H}_2\text{O})_4$ are shown in Figure 1. Previous studies^{28,32,44–46} have found that 4e possesses the lowest-energy geometry, and DF-MP2-F12/VDZ-F12 provided 4e as the lower-energy isomer. In this geometry, the length of the H bond that links water molecules is 1.760 Å, with a 129.27° distortion changing the geometry from 2D to 3D. The isomer possesses canonical geometry, with the four water molecules individually bound to each hydrogen atom on the ammonium. A previous work²⁹ found that $\text{Li}^+(\text{H}_2\text{O})_4$ and $\text{Na}^+(\text{H}_2\text{O})_4$ have similar lowest-energy geometries. The geometry of 4b has the lowest energy, and thus, it is the most stable structure. In 4a, the water molecule is linked to the other water molecule by H bond with a length of 1.683 Å. The geometry of 4c evolved from isomer 3b capped with one water molecule and linked to one water molecule, which is similar to the isomer of the $\text{H}_3\text{O}^+(\text{H}_2\text{O})_4$ cluster²⁹ and pure water cluster.⁴⁸ However, we obtain a special geometry, 4d, that evolved from isomer 3a, forming a pentagon geometry, which resembles the geometry of pure water clusters in previous works.⁴⁹ A free-jet expansion experiment^{28,50} found three $\text{NH}_4^+(\text{H}_2\text{O})_4$ isomers, with a clear peak in the distribution with clusters of four and five water molecules being the most abundant, indicating that there may be a special symmetrical geometry; thus, 4e with T_d geometry is very likely to become a more stable structure.

For the case of $\text{NH}_4^+(\text{H}_2\text{O})_5$ (Figure 2), the basket-like geometry of 5a has the lowest energy at the PW91PW91/6-

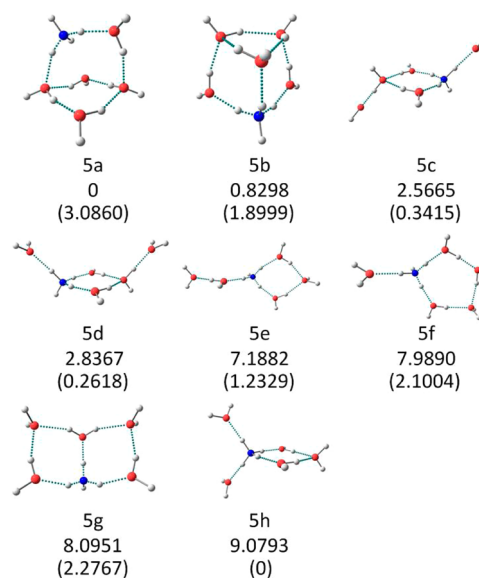


Figure 2. Optimized geometries of $\text{NH}_4^+(\text{H}_2\text{O})_5$. Relative energies are given in kcal/mol at the PW91PW91/6-311++G(3df,3pd) level, which are marked by na , nb , and nc , where the number n represents the cluster size; the energies at the DF-MP2/VDZ-F12 level are presented in parentheses. For ease of visualization, N atoms are shown in blue, and O and H atoms are shown in red and gray, respectively.

311++G(3df,3pd) level. According to the rule^{49,51–54} for the global minimum, the M_n geometry evolved from the lower-lying isomers of M_{n-1} ; thus, the geometry of 5a may evolve from some higher-energy isomers of $\text{NH}_4^+(\text{H}_2\text{O})_4$. In previous studies,^{33,44,46} 5h was found as a lowest-energy isomer, and DF-MP2-F12/VDZ-F12 provided 5h as the lowest-energy isomer, whereas PW91PW91/6-311+G(3df,3pd) provided 5h as the highest-energy isomer among the given eight structures. The geometry of 5h is also similar to the geometries of isomers of $\text{Li}^+(\text{H}_2\text{O})_5$ and $\text{Na}^+(\text{H}_2\text{O})_5$.²⁹ The trigonal prism geometry of Sb is the same as that of the water cluster for $(\text{H}_2\text{O})_6$,^{47,48,55,56} and some special isomers (5c, 5d, 5e, 5f, and 5g) were found. For 5c, which is derived from 4a, one water molecule is added to NH_4^+ , and the capped water molecule is situated on the opposite side. For 5d, which is derived from 4a and 4b, the capped water molecule is situated on the same side as in Figure 8. The 5e and 5f isomers possess a cyclic ring geometry with a line geometry, which is easy to develop into a cage. The booklike geometry of 5g is also found in the cluster of $(\text{H}_2\text{O})_6$ geometries.^{48,49,56}

As shown in Figure 3, the hexahedral geometry of isomer 6a of the $\text{NH}_4^+(\text{H}_2\text{O})_6$ cluster contains nine hydrogen bonds,

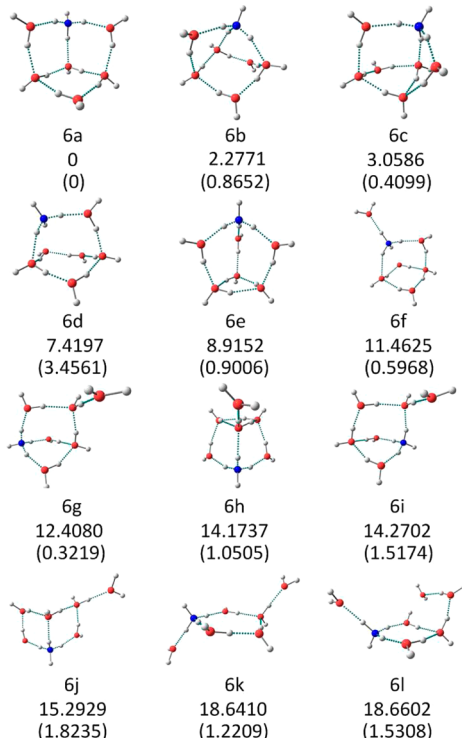


Figure 3. Optimized geometries of $\text{NH}_4^+(\text{H}_2\text{O})_6$. Relative energies are given in kcal/mol at the PW91PW91/6-311++G(3df,3pd) level, which are marked by na, nb, and nc, where the number n represents the cluster size; the energies at the DF-MP2/VDZ-F12 level are presented in parentheses. For ease of visualization, N atoms are shown in blue, and O and H atoms are shown in red and gray, respectively.

which is the largest number of hydrogen bonds that $\text{NH}_4^+(\text{H}_2\text{O})_6$ can form; this geometry was not found in previous studies.^{28,29,33,44,57,58} The geometries of 6b, 6c, 6d, and 6f suggest that isomer 5a may exist because 6b may be derived from 5a. In this case, one water molecule inserts into the arris of the 5a geometry, and an O–H bond develops between NH_4^+ and the water molecule. The geometry of 6d is similar to that of

the 6b isomer, but it does not develop O–H bonds. The geometry of 6e is very symmetrical, resembling a seismograph or a cage. This isomer may be formed from Sb by obtaining a water molecule; furthermore, we can conclude that the 6h is formed by Sb obtaining a water molecule. 6f evolves from 5a.

Because the number of possible isomers of $\text{NH}_4^+(\text{H}_2\text{O})_n$ increases considerably with increasing n (the number of water molecules), our calculations selected the top-12 lowest-lying optimized configurations of $\text{NH}_4^+(\text{H}_2\text{O})_7$, as shown in Figure 4.

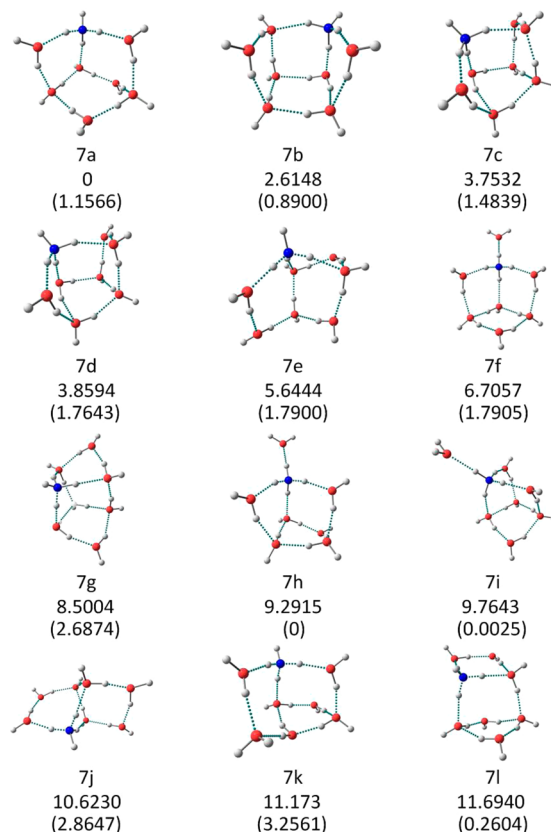


Figure 4. Optimized geometries of $\text{NH}_4^+(\text{H}_2\text{O})_7$. Relative energies are given in kcal/mol at the PW91PW91/6-311++G(3df,3pd) level, which are marked by na, nb, and nc, where the number n represents the cluster size; the energies at the DF-MP2-F12/VDZ-F12 level are presented in parentheses. For ease of visualization, N atoms are shown in blue, and O and H atoms are shown in red and gray, respectively.

The geometry of 7h is in good agreement with that previously found at the MP2 level,³³ and it was the global minimum at the DF-MP2-F12/VDZ-F12 level. The chairlike 7a with 10 hydrogen bonds is observed, which is derived from isomer 6a with a water molecule as the bottom of the chairlike geometry with ten H-bonds. The geometry of 7b resembles an armchair with 11 hydrogen bonds, and it is very symmetrical. The 7c and 7d isomers have two water molecules located on the side of NH_4^+ . The 7f isomer may evolve from 6a, linking a water molecule to NH_4^+ . The 7i and 7l isomers are derived from 6g, and the 7j isomers contain two pentagonal rings and one quadrangular ring.

For the $\text{NH}_4^+(\text{H}_2\text{O})_8$ geometries, we select 12 configurations that consist of NH_4^+ and eight water molecules, as shown in Figure 5. The 8a isomer with 13 H bonds is similar to the most stable isomer of the $(\text{H}_2\text{O})_9$ cluster.⁴⁹ The geometry of 8i is similar to the 8a configuration, but the capped water molecule

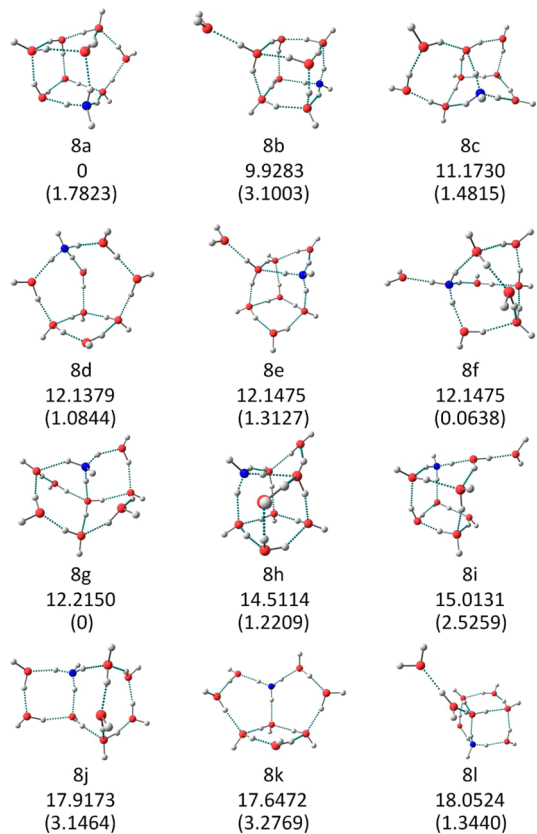


Figure 5. Optimized geometries of $\text{NH}_4^+(\text{H}_2\text{O})_8$. Relative energies are given in kcal/mol at the PW91PW91/6-311++G(3df,3pd) level, which are marked by *na*, *nb*, and *nc*, where the number *n* represents the cluster size; the energies at the DF-MP2-F12/VDZ-F12 level are presented in parentheses. For ease of visualization, N atoms are shown in blue, and O and H atoms are shown in red and gray, respectively.

results in a reaction with the 7b matrix. The geometries of 8a and 8i show that the reaction position and direction strongly affect the number of H bonds, and they adopt a different configuration than the parent isomer. The lantern-like geometry of 8b has 13 H bonds, which is close to 8a but higher in energy by 0.1029 eV. Although the position of the capped water molecule and resulting O–H bond are in opposite positions, the capped water molecule has a greater effect on the formation of H bonds. From the 8e isomer, we further confirm that the existence of the 8a isomer is reasonable. Some lower-energy geometries are shown in Figure 5, from which we found that the cyclic geometry consisting of six water molecules is more stable than that containing five water molecules that developed into a cyclic geometry. The isomer with a cage geometry is more stable than that consisting of a branch geometry; we extend this conclusion to many isomers, such as 8a being more stable than 8b and 8i, 8d being more stable than 8k, 8j being more stable than 8m, and so on.

For $\text{NH}_4^+(\text{H}_2\text{O})_9$, 9g was reported to be the lowest-energy isomer with 14 H bonds and four-membered rings in previous studies;³³ however, in our study, 9a is the lowest-energy isomer, with 13 H bonds at the PW91PW91/6-311++G(3df,3pd) level of theory. We found that many isomers are derived from 8a, such as 9a, 9b, 9f, and 9i. The 9c isomer possesses a symmetrical cage geometry with one triangle composed of three water molecules, three pentagons, and four quadrangles. An ammonium ion is shared by one pentagon and a

quadrangle, and 9c contains 15 H bonds and is higher in energy than 9a by 0.1379 eV. It is difficult to provide an example and explanation for the other isomers. In the clusters of $\text{NH}_4^+(\text{H}_2\text{O})_9$, there are 12 different cluster geometries, as shown in Figure 6.

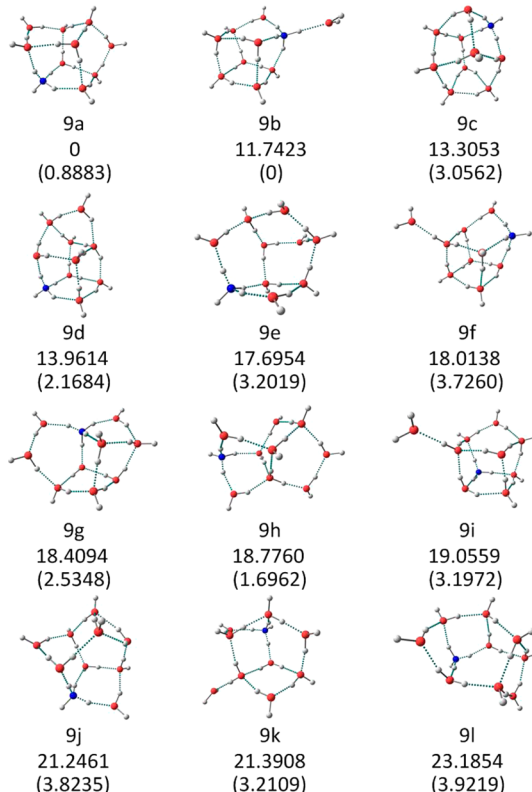


Figure 6. Optimized geometries of $\text{NH}_4^+(\text{H}_2\text{O})_9$. Relative energies are given in kcal/mol at the PW91PW91/6-311++G(3df,3pd) level, which are marked by *na*, *nb*, and *nc*, where the number *n* represents the cluster size; the energies at the DF-MP2-F12/VDZ-F12 level are presented in parentheses. For ease of visualization, N atoms are shown in blue, and O and H atoms are shown in red and gray, respectively.

We found that 10a is the lowest-energy isomer, resembling a room with a ridge and containing 16 H bonds. As shown in Figure 7, the geometry of 10a is very symmetrical. We do not know from which of the $\text{NH}_4^+(\text{H}_2\text{O})_9$ isomers that this geometry arises. The geometry of 10h is also very symmetrical, containing 11 H bonds. It is very difficult to describe the other geometries.

The geometries of the clusters strongly affect their properties. Comparing $M^+(\text{H}_2\text{O})_n$ (where *M* represents the alkali metal or water) clusters with $\text{NH}_4^+(\text{H}_2\text{O})_n$ clusters revealed that there may be some similarity between $\text{NH}_4^+(\text{H}_2\text{O})_n$ and $M^+(\text{H}_2\text{O})_n$. According to experience,^{49,51,53,54,59} the global minimum M_n geometry can typically be found from one of the low-lying isomers of M_{n-1} . Some routes for the evolution of $\text{NH}_4^+(\text{H}_2\text{O})_n$ (*n* = 1–6) clusters are presented in Figure 8, and we provide some discussion about the reaction between the matrix and water molecules. As the size of the cluster increases, the evolution route becomes more complex and varies. Some lower-energy isomers will lead to higher-energy isomers, while at the same time, some lower-energy isomers will be derived from higher-energy matrix isomers due to the calculation uncertainty. We can also observe that a matrix can produce

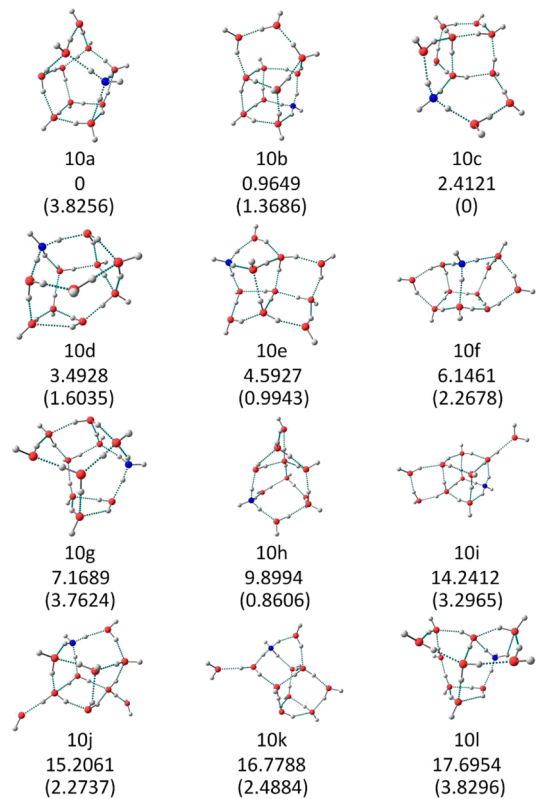


Figure 7. Optimized geometries of $\text{NH}_4^+(\text{H}_2\text{O})_{10}$. Relative energies are given in kcal/mol at the PW91PW91/6-311++G(3df,3pd) level, which are marked by na , nb , and nc , where the number n represents the cluster size; the energies at the DF-MP2-F12/VDZ-F12 level are presented in parentheses. For ease of visualization, N atoms are shown in blue, and O and H atoms are shown in red and gray, respectively.

different next-generation isomers. From the evolution of the geometries, we can determine whether some of the isomers are reasonable. The direction and position of the capped water significantly affect the geometry and energy of the generated isomer, and this phenomenon can be explained by observing 8a and 8i in Figure 5.

When $n < 3$, $\text{NH}_4^+(\text{H}_2\text{O})_n$ tends to form the longest possible linear hydrogen bonds, but the geometry of $\text{NH}_4^+(\text{H}_2\text{O})_n$ tends to change from linear to circular. When $n \geq 3$, the water molecules tend to form a ring or a symmetric or opened cage

geometry. When $n = 8$, the clusters begin to form a closed-cage geometry through intermolecular hydrogen bonds, thereby greatly strengthening the intermolecular interaction. According to previous studies,⁴⁸ due to the nonadditive components of the binding energy, the geometries are different.

B. Relative Stabilities and Thermodynamics of $\text{NH}_4^+(\text{H}_2\text{O})_n$ Formation. The enthalpies, entropies, and resulting Gibbs free energies, which are the properties that determine the nucleation rates, are calculated using the equilibrium/optimized geometries and calculated vibrational frequencies. The parameters for characterizing the thermodynamics of $\text{NH}_4^+(\text{H}_2\text{O})_n$ ($n = 1-10$) clusters are the $\Delta E + \text{ZPE}$ (kcal/mol), ΔH (kcal/mol), and ΔG (kcal/mol) energies for incremental reactions of a water molecule with successive hydrate clusters, where $\Delta E + \text{ZPE}$ is the binding energy with zero-point correction, ΔH is the enthalpies and ΔG is the Gibbs free energy. To study the influent of zero-point correction, we compared the relative energies of with ZPE corrections with the relative energies without ZPE corrections; the comparison is in Table S14 in the Supporting Information. The results show that the ZPE corrections changes the relative order of isomers, for example the 3a not to be global minima without ZPE, but adding ZPE corrections makes 3a not the global minimum. And 4a is more stable than 4e without ZPE, but the ZPE corrections change the order. The weights of the global minimum and other local minima become competitive as the temperature increases. We can gain the conclusion in Figures 12 and 13, for example, 8f is more stable than 8a from the view of Gibbs free energy. Different nucleation pathways are controlled by two key factors: the thermodynamic stability of the prenucleation clusters and the concentrations of the reacting species. Thus, we calculate the thermodynamic parameters on the basis of the derived lowest-energy isomers, in which the atmospheric nucleation precursor and hydration affect the stability, mobility and lifetime of ions. For $\text{NH}_4^+(\text{H}_2\text{O})_n$ clusters, the successive binding energy (ΔE) can be calculated as follows:

$$\Delta E = E_{\text{NH}_4^+(\text{H}_2\text{O})_n} - E_{\text{NH}_4^+(\text{H}_2\text{O})_{n-1}} - E_{\text{H}_2\text{O}} \quad (1)$$

Table 1 presents the enthalpies and binding energies with zero-point ($\Delta E + \text{ZPE}$) corrections associated with reactions among clusters of $\text{NH}_4^+(\text{H}_2\text{O})_{n-1}$ and water monomer, in which the most stable isomer changes as the number of water molecules increases. Figure 9 (left) depicts the successive

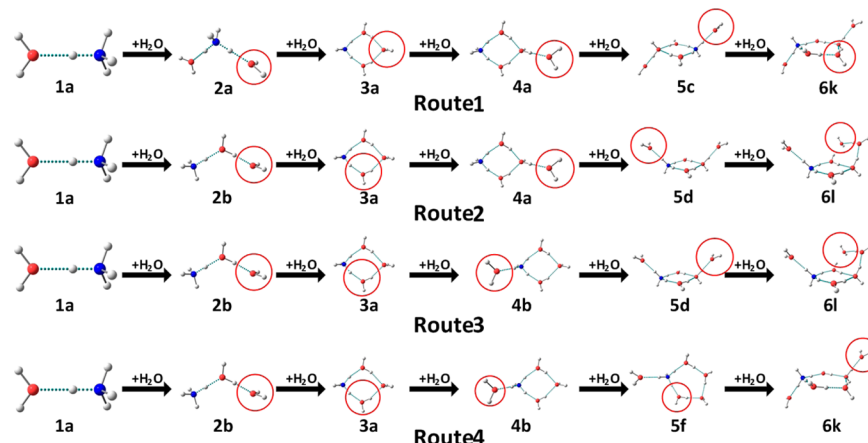


Figure 8. Structural evolutions of the clusters $\text{NH}_4^+(\text{H}_2\text{O})_n$ ($n = 1-6$). The red rings indicate the added water molecules.

Table 1. $\Delta E + ZPE$ (kcal/mol), ΔH (kcal/mol), and ΔG (kcal/mol) Changes Associated with Reactions among Clusters Composed of Atmospheric Precursors (Ammonium and Water) Calculated at $T = 298$ K

N	PW91PW91/6-311++G(3df,3pd)			DF-MP2-F12/VDZ-F12			MP2/CBS		exptl 298 K
	ΔE	ΔH	ΔG	ΔE	ΔH	ΔG	ΔE	ΔH	ΔG^0
1	-20.1	-21.3	-12.3	-18.9	-20.1	-11.1	-18.9	-13.8	-13.1
2	-15.4	-15.2	-9.4	-15.4	-15.7	-8.1	-15.3	-7.5	-7.6
3	-10.8	-12.1	-0.3	-13.1	-12.5	-7.7	-13.0	-5.5	-6.0
4	-11.9	-12.2	-5.1	-11.1	-11.0	-3.4	-11.2	-4.9	-4.0
5	-6.8	-8.7	5.1	-10.0	-11.1	-0.8	-9.9	-1.2	-2.8
6	-12.6	-13.2	-4.1	-9.1	-11.5	3.9	-10.6	0.7	-2.5
7	-10.3	-11.0	-1.4	-10.2	-10.8	-1.7	-6.6	2.5	
8	-7.0	-9.0	4.6	-8.5	-10.1	2.5	-8.6	-0.7	
9	-11.6	-12.3	-2.8	-10.3	-10.9	-1.6	-11.4	1.3	
10	-5.5	-6.9	4.6	-7.3	-8.3	1.2	-9.7	-0.4	

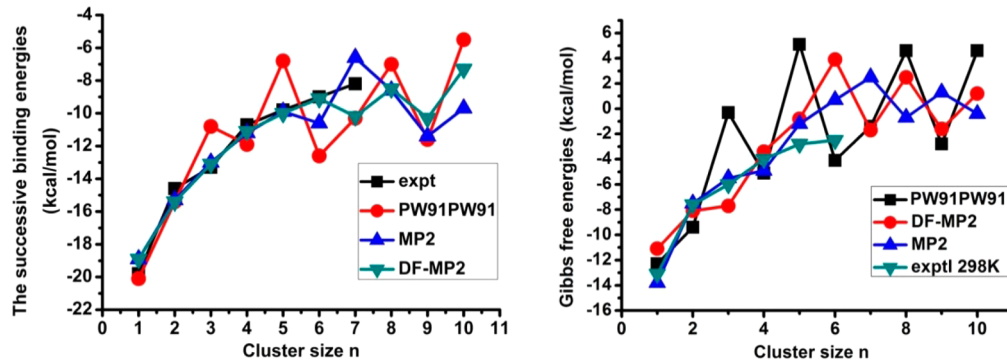


Figure 9. Successive binding energies with zero-point correction ($\Delta E + ZPE$) and the Gibbs free energies associated with the formation of $\text{NH}_4^+(\text{H}_2\text{O})_n$ ($n = 1-10$) at the PW91PW91/6-311++G(3df,3pd) level of theory, the DF-MP2-F12/VDZ-F12 level of theory, and MP2/CBS//MP2/6-31G* level of theory.

binding energies for $\text{NH}_4^+(\text{H}_2\text{O})_n$ ($n = 1-10$) as a function of the cluster size, n . As shown in Figure 9, there are some differences in the convergence of the binding energy at the PW91PW91/6-311++G(3df,3pd) level of theory, the DF-MP2-F12/VDZ-F12 level of theory and MP2/CBS//MP2/6-31G* level of theory; however, the calculations are in very good agreement with the experimental values of the successive binding energy⁴⁶ at the DF-MP2-F12/VDZ-F12 level of theory than those values calculated at PW91PW91/6-311++G(3df,3pd) level of theory and MP2/CBS//MP2/6-31G* level of theory. Figure 9 shows that convergence of the binding energy is not monotonic. When $n = 1-4$, as the number of water molecules increases, the average polarization of ammonium with water molecules increases, leading to a gradual increase in the binding energy. When n is greater than 4, because the first hydrated layer of ammonium and water molecules is saturated, the ammonium ion reacts with the outer first hydrated layer, and water molecule polarization is very weak. The contribution of binding energy comes primarily from the interaction between water molecules. When $n = 5-6$, the binding energy continues to increase, which suggests that the interaction between water molecules is weaker than the interaction between ammonium and water molecules. When $n = 7$, the binding energy begins to decrease, and when $n = 8$, the binding energy suddenly increases. At this point, clusters began to form with a closed-cage geometry through intermolecular hydrogen bonds, thereby greatly strengthening the intermolecular interaction. When $n = 9$, the binding energy begins to decrease again; however, when $n = 10$, the binding

energy begins to increase again. The increase in the number of H bonds further strengthens the intermolecular interaction.

For $\text{NH}_4^+(\text{H}_2\text{O})_n$ clusters, the Gibbs free energy can be calculated as follows:

$$\Delta G = G_{\text{NH}_4^+(\text{H}_2\text{O})_n} - G_{\text{NH}_4^+(\text{H}_2\text{O})_{n-1}} - G_{\text{H}_2\text{O}} \quad (2)$$

Changes in the Gibbs free energy are associated with reactions among clusters composed of $\text{NH}_4^+(\text{H}_2\text{O})_{n-1}$ and water molecules. Figure 9 (right) depicts the Gibbs free energies for $\text{NH}_4^+(\text{H}_2\text{O})_n$ ($n = 1-10$) as a function of the cluster size, n . The calculations are in good agreement with experimental values of the Gibbs free energies at the DF-MP2-F12/VDZ-F12 level and MP2/CBS level of theory. In Earth's atmosphere, the atmospherically relevant temperature ranges from 200 to 300 K depending on the altitude; thus, we investigated the Gibbs free energy for the formation of $\text{NH}_4^+(\text{H}_2\text{O})_n$ ($n = 1-10$) clusters at different temperatures (200–300 K). The calculated successive binding energy is in very good agreement with the experimental values at the DF-MP2-F12/VDZ-F12 level. Thus, we adopt the Gibbs free energy values at the DF-MP2-F12/VDZ-F12 level. The most stable isomer changes as the number of water molecules increases. Figure 10 presents the Gibbs free energies for $\text{NH}_4^+(\text{H}_2\text{O})_n$ ($n = 1-10$) as a function of the cluster size n at different temperatures. As shown, the Gibbs free energies have similar tendencies at different temperatures. When $n = 1-6$, as the number of water molecules in $\text{NH}_4^+(\text{H}_2\text{O})_n$ increases, the Gibbs free energy values increase, indicating that it becomes increasingly difficult for the $\text{NH}_4^+(\text{H}_2\text{O})_{n-1}$ cluster to gain a water molecule. When $n = 6$, the value of the Gibbs free energy

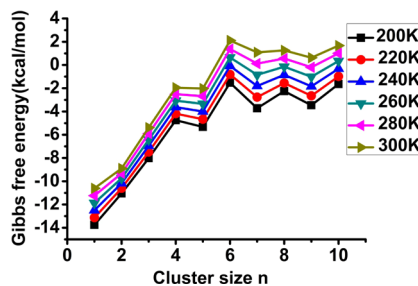


Figure 10. Gibbs free energies associated with the formation of $\text{NH}_4^+(\text{H}_2\text{O})_n$ ($n = 1\text{--}10$) at 200–300 K.

is negative at temperatures below 240 K, and the stepwise addition of water molecules is favorable; however, when the temperature is greater than 240 K, the value of the Gibbs free energy is positive, indicating that the reaction to cap $\text{NH}_4^+(\text{H}_2\text{O})_5$ with a water molecule to produce $\text{NH}_4^+(\text{H}_2\text{O})_6$ is very difficult. When $n > 6$, the value of the Gibbs free energy begins to decrease, and when the temperature is greater than 260 K, the value of the Gibbs free energy is negative, indicating that the stepwise addition of water molecules is favorable. The calculated Gibbs free energies for the formation of $\text{NH}_4^+(\text{H}_2\text{O})_n$ ($n = 1\text{--}10$) clusters at different temperatures (200–300 K) predict that the formation of $\text{NH}_4^+(\text{H}_2\text{O})_n$ ($n = 1\text{--}10$) clusters is favorable in the colder regions of the troposphere; thus, the sedimentation phenomenon may be able to explain why some clusters can be detected at lower altitudes.

C. Hydration at Different Temperatures and Humidities. It is interesting to determine the actual concentrations of the various hydrated clusters of ammonium under specific realistic atmospheric conditions. The quantum chemistry method for predicting the actual concentration is through a stepwise building of the cluster by adding a water molecule to an existing hydrate, for example, by adding a water molecule to each $\text{NH}_4^+(\text{H}_2\text{O})_{n-1}$ cluster to form $\text{NH}_4^+(\text{H}_2\text{O})_n$. The concentration of each hydrate depends on the concentration of the $\text{NH}_4^+(\text{H}_2\text{O})_{n-1}$ hydrate precursor, the concentration of water, and thermodynamics.^{60,61} To draw further conclusions, we need to know how the number of water molecules in the clusters is affected by the relative humidity.

Considering the relative concentration of ammonium-hydrate, we used the number concentration of hydrate, which was obtained according to the method reported by Noppel et al.¹³ The equations that we utilized are as follows:

$$\rho(1,n) = K_1 K_2 \cdots K_n \left(\frac{\rho_{\text{water}}^{\text{free}}}{\rho} \right)^n \rho_{\text{NH}_4^+}^{\text{free}} \quad (3)$$

where K_m are the equilibrium constants^{62,63} and $\rho_{\text{water}}^{\text{free}}$ is the free monomer concentration of water.

$$K_m = e^{-\Delta G_m / RT} \quad (4)$$

$$\rho_{\text{water}}^{\text{free}} = \frac{S}{k_B T} P_{\text{water}}^{\text{eq}} \quad (5)$$

We can indirectly obtain the concentration from the equilibrium constant K_m . The equilibrium constant K_m for the formation of the clusters from the respective monomers is given by the standard free energies ΔG , where T is the temperature, R is the molar gas constant, S is defined as the saturation ratio, k_B is the Boltzmann constant, and $P_{\text{water}}^{\text{eq}}$ is the saturation vapor pressure of water. The saturation vapor pressure of water vapor is given by Seinfeld and Pandis,⁶⁴ and the saturated water vapor pressures at different temperatures are shown in Table S1 in the Supporting Information.

The reference concentration ρ can be determined in terms of some reference pressure P (here, $P = 1$ atm), as follows:

$$\rho = \frac{P}{k_B T} \quad (6)$$

where P is the reference pressure (here, $P = 1$ atm), k_B is the Boltzmann constant, and T is the temperature. To determine the actual concentrations of the various hydrated clusters of ammonium under a given realistic atmospheric condition, we should first know the relative fractions of the different hydrates of the cluster cores. The relative concentrations of some m -hydrates were reported⁵⁹ by Weber⁶² and co-workers.⁶¹ To assess the extent of ammonium hydration under different circumstances, we calculated the hydrate distributions for $\text{NH}_4^+(\text{H}_2\text{O})_n$ ($n = 0\text{--}10$) at different relative humidities (RH) and temperatures (standard for different altitudes), and the hydrate distributions are presented in Figure 11. Three relative humidity values (20%, 50%, and 80%) at 298.15 K are shown in Figure 11, as well as three values of relative temperature (280, 298.15, and 300 K) at a relative humidity of 50%. The saturation vapor pressure of water is influenced by the relative temperatures. A decreasing temperature decreases the absolute water concentration, but the hydrate distribution at a constant RH does not significantly change with changing temperature.

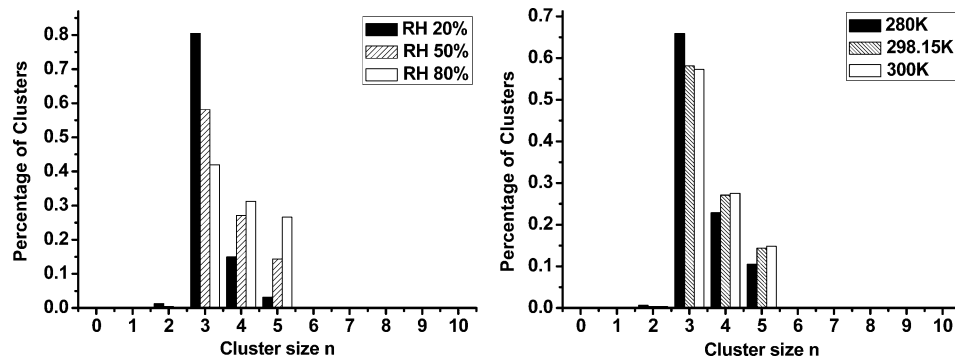


Figure 11. Hydrate distributions of $\text{NH}_4^+(\text{H}_2\text{O})_n$ ($n = 1\text{--}10$) clusters (left) at three different relative humidities when $T = 298.15$ K and (right) at three different relative temperatures when $\text{RH} = 50\%$.

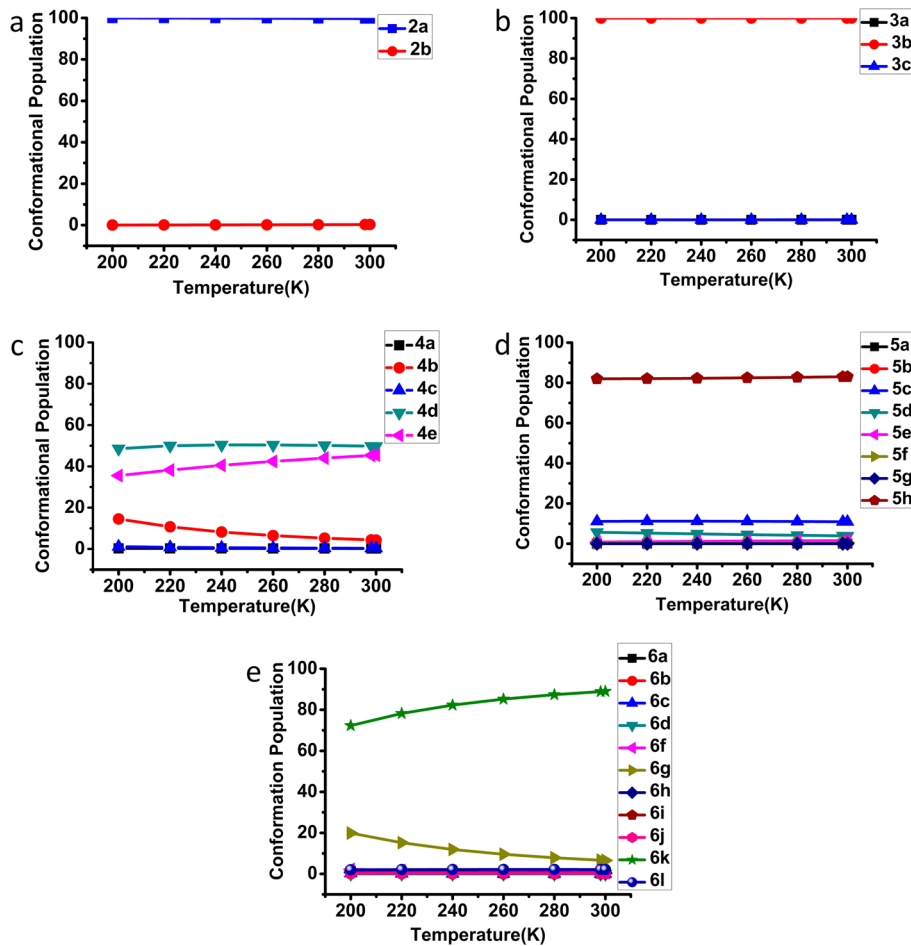


Figure 12. Conformational population of different isomers with the same sizes as a function of the temperature variance.

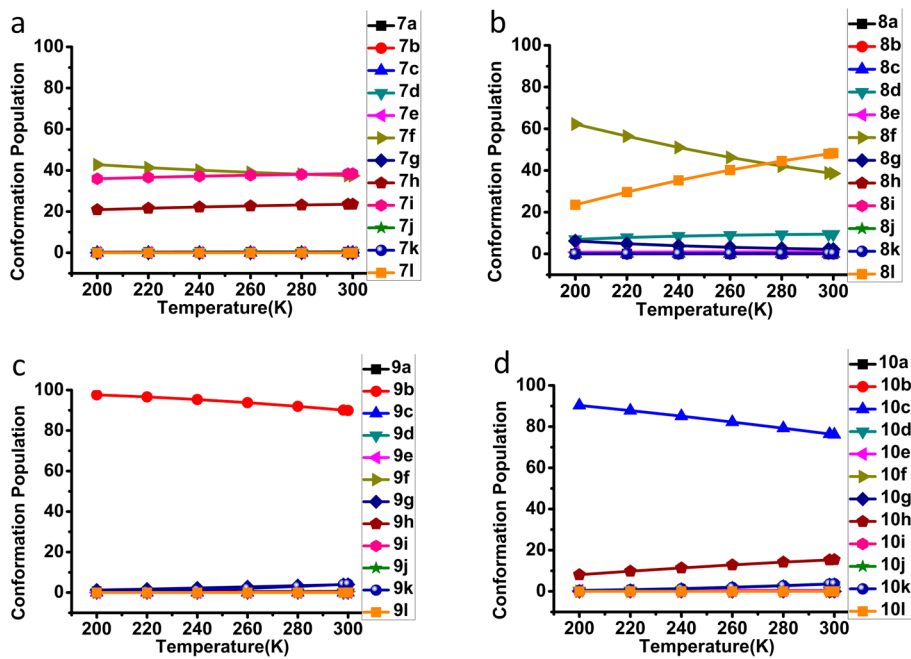


Figure 13. Conformational population depending on the temperature variance.

The percentages of $\text{NH}_4^+(\text{H}_2\text{O})_3$ are the highest at different humidities and temperatures, as shown in Figure 11. This behavior can be explained by the structure: the geometry

changed from 2D to 3D, leading to stronger bonding. On the other hand, the relative humidity and temperature change, which implies that $\text{NH}_4^+(\text{H}_2\text{O})_3$ clusters are favorable at lower

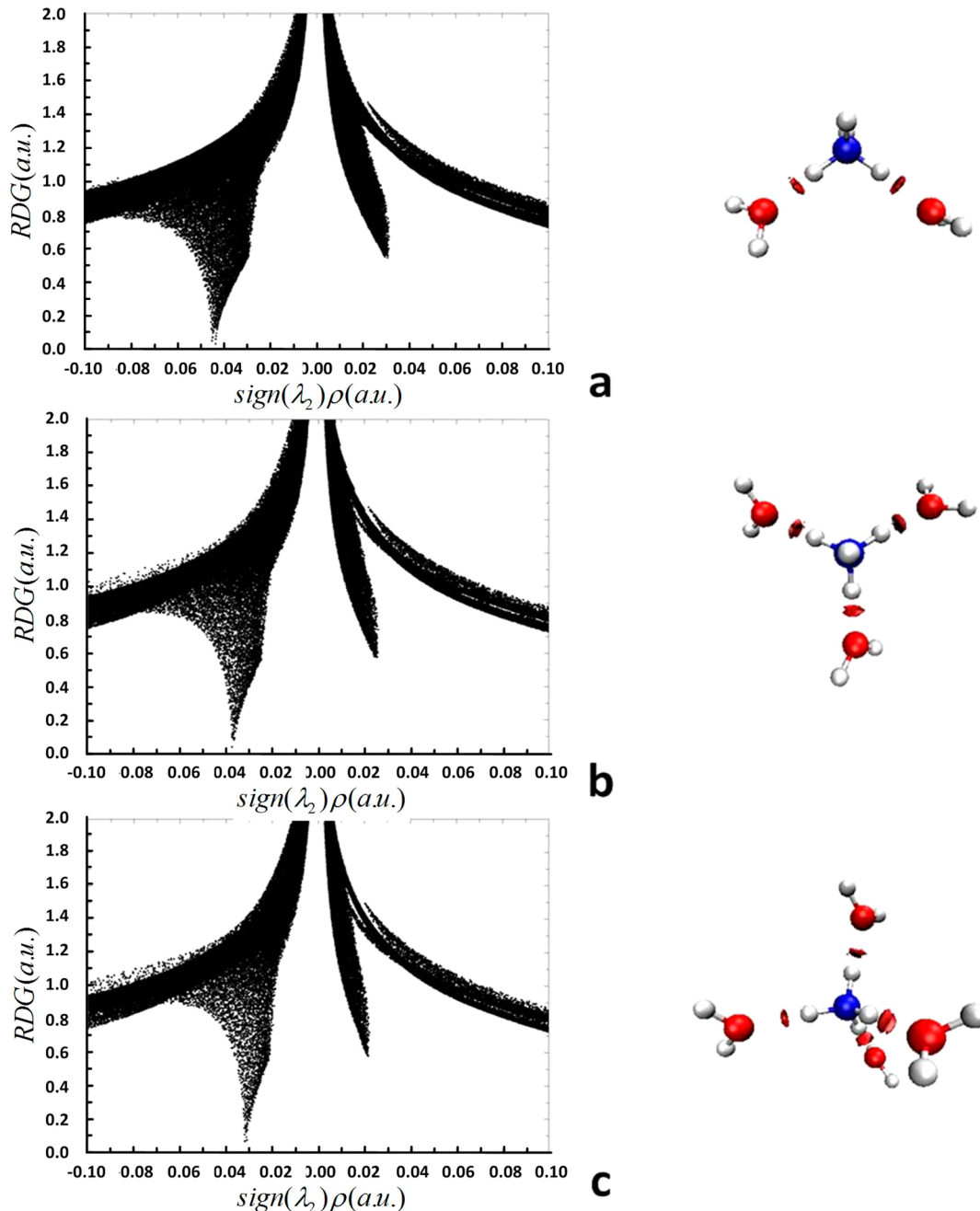


Figure 14. Noncovalent interactions (NCI) analysis.

values of relative humidity ($\text{RH} < 50\%$) and lower relative temperatures ($T < 298.15 \text{ K}$). $\text{NH}_4^+(\text{H}_2\text{O})_4$ and $\text{NH}_4^+(\text{H}_2\text{O})_5$ clusters are favorable at higher values of relative humidity and higher relative temperatures, but the percentage would decrease as the clusters grow. This phenomenon can most likely be explained by considering the dipole–dipole interaction between the cluster and water: as the clusters grow, the dipole–dipole interaction would become weaker.

D. Temperature Dependence of the Conformational Population and Boltzmann-Averaged Gibbs Free Energies. The Global minimum has the largest population in the ensemble of energetically accessible conformers at 0 K. However, in Earth's atmosphere, the atmospherically relevant temperature ranges from 200 to 300 K, and the temperature effects are an important parameter that can contribute to

changing the stability order of isomers. In addition, because the cluster systems become larger and the configurations become more complex, the energy differences between the global minimum and other local minima become smaller; thus, the contributions from all of the lower-energy isomers might be important. Therefore, the coupling effects on the lower-energy isomer contributions and temperature effects were investigated, which could provide a more accurate picture of the relative stabilities of the isomers.

To determine the contribution of each low-energy isomer, we used the Boltzmann-averaged Gibbs free energy, according to the Boltzmann factors reported by Temelso et al.⁶⁰ To study the flatness of the potential energy surface of $\text{NH}_4^+(\text{H}_2\text{O})_n$ ($n = 2–10$), we used the following equations:

$$\eta_{ni} = \frac{e^{-\Delta\Delta G_T^{ni}/k_B T}}{\sum_{ni} e^{-\Delta\Delta G_T^{ni}/k_B T}} \quad (7)$$

$$\Delta G_T^n = \sum_{ni} \eta_{ni} \Delta G_T^{ni} \quad (8)$$

where

$$\Delta G_n^i = G_n^i - G^{\text{SA}} - nG^{\text{W}} \quad (9)$$

$$\Delta\Delta G_n^i = \Delta G_n^i - \min\{\Delta G_n^i\} \quad (10)$$

The dependence of the conformational population on the temperature variance is shown in Figures 12 and 13. The percentage of 2a, 3b, and 5h is greater than 80% with temperature changes between 200 and 300 K, indicating that these structures are more stable; these structures were found in the experiment. The conformational population of 4d and 6k became larger as the temperature increased, whereas that of 4b and 6g decreased. In general, as the systems become larger and the configurations become more complex, the energetic difference between the global minimum and local minima becomes smaller. As shown in Figures 13a and 13b, and the weight of 8l is greater than that of 8f when the temperature is greater than 280 K. However, as the temperature increases, although the weights of 9b and 10c slightly decrease, the gap in the conformation population among 9b, 10c, and others remains larger, indicating that the clusters potential energy surfaces (PES) of same components at different sizes are complex and different.

E. Analysis of Noncovalent Interactions (NCI). The noncovalent interaction (NCI) index is based on the relationship between the electron density and the reduced density gradient. The main purpose of this method is to highlight the weak interaction area of the system. To determine the strengths of the noncovalent interactions and the covalent interactions, we used the reduced density gradient function (RDG), which was obtained according to the method reported by Yang and co-workers.^{65,66} According to the definition of the RDG by Yang and co-workers, we can determine whether the interaction is attractive or nonbonding. Therefore, the NCI index is a useful tool for distinguishing and visualizing different types of noncovalent interactions in real space. The plots of the reduced density gradient versus the electron density multiplied by the sign of the second Hessian eigenvalue (above) and isosurfaces generated for $\text{NH}_4^+(\text{H}_2\text{O})_n$ ($n = 2-4$) are shown in Figure 14.

The value (below zero) of electron density multiplied by the sign of the second Hessian eigenvalue increases gradually with increasing n , indicating that these interactions are becoming weaker in the sequence, which is in good agreement with the binding energy calculations. According to the NCI analysis, the influence of NH_4^+ gradually weakens in the sequence.

IV. CONCLUSION

In the paper, the formation of $\text{NH}_4^+(\text{H}_2\text{O})_n$ ($n = 1-10$) was theoretically investigated. New thermochemical data, including successive binding energies with zero-point correction and Gibbs free energies, have been reported, and the geometries and evolution of geometries for $\text{NH}_4^+(\text{H}_2\text{O})_n$ clusters have been presented. An abundance of $\text{NH}_4^+(\text{H}_2\text{O})_n$ under ambient conditions has also been reported. The results of the present study lead us to the following conclusions:

- (a) Combining the basin-hopping method with density functional theory provides an economic and effective method for searching the global minimum and optimized isomers of molecular clusters of $\text{NH}_4^+(\text{H}_2\text{O})_n$.
- (b) On the basis of the evolution of $\text{NH}_4^+(\text{H}_2\text{O})_n$ ($n = 1-6$) clusters, we drew the following conclusions: (1) As the size of the cluster increases, the evolution pathways become more complex and vary, and some lower-energy isomers were derived from a higher-energy matrix isomer. (2) The direction and position of the capped water significantly influence the geometry and energy of the generated isomer.
- (c) As the size of the $\text{NH}_4^+(\text{H}_2\text{O})_n$ cluster increases, the reaction among clusters composed of $\text{NH}_4^+(\text{H}_2\text{O})_{n-1}$ and water monomer becomes increasingly difficult, but nucleation is favorable in the colder regions of the troposphere.
- (d) The relatively larger $\text{NH}_4^+(\text{H}_2\text{O})_n$ clusters are favorable under higher-humidity conditions, but the relatively smaller clusters are more favorable in lower-humidity environments.
- (e) The potential energy surfaces (PES) of clusters with the same components and different sizes are complex and different.
- (f) As the size of the clusters increases, noncovalent interactions weaken in the sequence.

The particle formation events observed in the experiment and in the atmosphere may involve multiple-component nucleation processes. Further research is needed to extend the present study to larger nucleation clusters that contain more water molecules and other species so that we can systematically study cluster formation and evolution and calculate the concentrations of different clusters during combined field observation tests.

ASSOCIATED CONTENT

Supporting Information

Saturated water vapor pressures, Cartesian coordinates, and relative energies. This material is available free of charge via the Internet at <http://pubs.acs.org>.

AUTHOR INFORMATION

Corresponding Author

*W. Huang. E-mail: huangwei6@ustc.edu.cn.

Notes

The authors declare no competing financial interest.

ACKNOWLEDGMENTS

The study was supported by grants from the National Natural Science Foundation of China (Grant No. 21403244 and 21133008), the National High Technology Research and Development Program of China (863 Program) (Grant No. 2014AA06A501). "Interdisciplinary and Cooperative Team" of CAS. Acknowledgement is also made to the "Thousand Youth Talents Plan". The computation was performed in EMSL, a national scientific user facility sponsored by the department of Energy's Office of Biological and Environmental Research and located at Pacific Northwest National Laboratory (PNNL). PNNL is a multiprogram national laboratory operated for the DOE by Battelle. Part of the computation was performed at the Supercomputing Center of USTC.

■ REFERENCES

- (1) Li, Q.; An, X.; Gong, B.; Cheng, J. Cooperativity between OH···O and CH···O Hydrogen Bonds Involving Dimethyl Sulfoxide-H₂O-H₂O Complex. *J. Phys. Chem. A* **2007**, *111*, 10166–10169.
- (2) Dudowicz, J.; Douglas, J. F.; Freed, K. F. Self-Assembly by Mutual Association: Basic Thermodynamic Properties. *J. Phys. Chem. B* **2008**, *112*, 16193–16204.
- (3) Kerminen, V.-M.; Lihavainen, H.; Komppula, M.; Viisanen, Y.; Kulmala, M. Direct Observational Evidence Linking Atmospheric Aerosol Formation and Cloud Droplet Activation. *Geophys. Res. Lett.* **2005**, *32*, L14803 DOI: 10.1029/2005GL023130.
- (4) Saxon, A.; Diaz-Sanchez, D. Air Pollution and Allergy: You Are What You Breathe. *Nat. Immunol.* **2005**, *6*, 223–226.
- (5) Kennedy, I. M. The Health Effects of Combustion-Generated Aerosols. *Proc. Combust. Inst.* **2007**, *31*, 2757–2770.
- (6) Weissenbach, J.; Gyapay, G.; Dib, C.; Vignal, A.; Morissette, J.; Millasseau, P.; Vaysseix, G.; Lathrop, M. A Second-Generation Linkage Map of the Human Genome. *Nature* **1992**, *359*, 794–801.
- (7) Zhang, R. Getting to the Critical Nucleus of Aerosol Formation. *Science* **2010**, *328*, 1366–1367.
- (8) Zhang, R.; Khalizov, A.; Wang, L.; Hu, M.; Xu, W. Nucleation and Growth of Nanoparticles in the Atmosphere. *Chem. Rev.* **2012**, *112*, 1957–2011.
- (9) Kim, J.; Lee, H. M.; Suh, S. B.; Majumdar, D.; Kim, K. S. Comparative Ab Initio Study of the Structures, Energetics and Spectra of X⁻(H₂O)_n (n = 1–4) [X = F, Cl, Br, I] Clusters. *J. Chem. Phys.* **2000**, *113*, 5259–5272.
- (10) Temelso, B.; Phan, T. N.; Shields, G. C. Computational Study of the Hydration of Sulfuric Acid Dimers: Implications for Acid Dissociation and Aerosol Formation. *J. Phys. Chem. A* **2012**, *116*, 9745–9758.
- (11) Kulmala, M.; Vehkämäki, H.; Petäjä, T.; Dal Maso, M.; Lauri, A.; Kerminen, V.-M.; Birmili, W.; McMurry, P. H. Formation and Growth Rates of Ultrafine Atmospheric Particles: A Review of Observations. *J. Aerosol Sci.* **2004**, *35*, 143–176.
- (12) Chen, D.-R.; Pui, D. Y.; Hummes, D.; Fissan, H.; Quant, F.; Sem, G. Design and Evaluation of a Nanometer Aerosol Differential Mobility Analyzer (Nano-DMA). *J. Aerosol Sci.* **1998**, *29*, 497–509.
- (13) Noppel, M.; Vehkämäki, H.; Kulmala, M. An Improved Model for Hydrate Formation in Sulfuric Acid–Water Nucleation. *J. Chem. Phys.* **2002**, *116*, 218–228.
- (14) Yu, F. Improved Quasi-Unary Nucleation Model for Binary H₂SO₄-H₂O Homogeneous Nucleation. *J. Chem. Phys.* **2007**, *127*, 054301.
- (15) Napari, I.; Noppel, M.; Vehkämäki, H.; Kulmala, M. Parametrization of Ternary Nucleation Rates for H₂SO₄-NH₃-H₂O Vapors. *J. Geophys. Res.* **2002**, *107*, 4381 DOI: 10.1029/2002JD002132..
- (16) Yu, F. The Effect of Ammonia on New Particle Formation: A Kinetic H₂SO₄-H₂O-NH₃ Nucleation Model Constrained by Laboratory Measurements. *J. Geophys. Res.* **2006**, *111*, D01204 DOI: 10.1029/2005JD005968.
- (17) Yu, F.; Turco, R. P. Ultrafine Aerosol Formation Via Ion-Mediated Nucleation. *Geophys. Res. Lett.* **2000**, *27*, 883–886.
- (18) Lovejoy, E.; Curtius, J.; Froyd, K. Atmospheric Ion-Induced Nucleation of Sulfuric Acid and Water. *J. Geophys. Res.* **2004**, *109*, D08204 DOI: 10.1029/2003JD004460.
- (19) Yu, F. From Molecular Clusters to Nanoparticles: Second-Generation Ion-Mediated Nucleation Model. *Atmos. Chem. Phys.* **2006**, *6*, 5193–5211.
- (20) Zhang, R.; Suh, I.; Zhao, J.; Zhang, D.; Fortner, E. C.; Tie, X.; Molina, L. T.; Molina, M. J. Atmospheric New Particle Formation Enhanced by Organic Acids. *Science* **2004**, *304*, 1487–1490.
- (21) Nadykto, A. B.; Yu, F. Strong Hydrogen Bonding between Atmospheric Nucleation Precursors and Common Organics. *Chem. Phys. Lett.* **2007**, *435*, 14–18.
- (22) Zhao, J.; Khalizov, A.; Zhang, R.; McGraw, R. Hydrogen-Bonding Interaction in Molecular Complexes and Clusters of Aerosol Nucleation Precursors. *J. Phys. Chem. A* **2009**, *113*, 680–689.
- (23) Walker, J.; Whitall, D. R.; Robarge, W.; Paerl, H. W. Ambient Ammonia and Ammonium Aerosol across a Region of Variable Ammonia Emission Density. *Atmos. Environ.* **2004**, *38*, 1235–1246.
- (24) Prenni, A. J.; DeMott, P. J.; Kreidenweis, S. M. Water Uptake of Internally Mixed Particles Containing Ammonium Sulfate and Dicarboxylic Acids. *Atmos. Environ.* **2003**, *37*, 4243–4251.
- (25) Sutton, M.; Milford, C.; Dragosits, U.; Place, C.; Singles, R.; Smith, R.; Pitcairn, C.; Fowler, D.; Hill, J.; ApSimon, H. Dispersion, Deposition and Impacts of Atmospheric Ammonia: Quantifying Local Budgets and Spatial Variability. *Environ. Pollut.* **1998**, *102*, 349–361.
- (26) McCubbin, D. R.; Apelberg, B. J.; Roe, S.; Divita, F. Livestock Ammonia Management and Particulate-Related Health Benefits. *Environ. Sci. Technol.* **2002**, *36*, 1141–1146.
- (27) Wayne, R. P. *Chemistry of Atmospheres*; Oxford University Press: Oxford, U.K., 1991.
- (28) Wang, Y.-S.; Chang, H.-C.; Jiang, J.-C.; Lin, S. H.; Lee, Y. T.; Chang, H.-C. Structures and Isomeric Transitions of NH₄⁺(H₂O)_{3–6}: From Single to Double Rings. *J. Am. Chem. Soc.* **1998**, *120*, 8777–8788.
- (29) Lee, H. M.; Tarakeshwar, P.; Park, J.; Kolaski, M. R.; Yoon, Y. J.; Yi, H.-B.; Kim, W. Y.; Kim, K. S. Insights into the Structures, Energetics, and Vibrations of Monovalent Cation-(Water)_{1–6} Clusters. *J. Phys. Chem. A* **2004**, *108*, 2949–2958.
- (30) Karthikeyan, S.; Singh, J. N.; Park, M.; Kumar, R.; Kim, K. S. Structures, Energetics, Vibrational Spectra of NH₄⁺(H₂O)_n (n = 4, 6) Clusters: Ab Initio Calculations and First Principles Molecular Dynamics Simulations. *J. Chem. Phys.* **2008**, *128*, 244304.
- (31) Douady, J.; Calvo, F.; Spiegelman, F. Structure, Stability, and Infrared Spectroscopy of (H₂O)_n NH₄⁺ Clusters: A Theoretical Study at Zero and Finite Temperature. *J. Chem. Phys.* **2008**, *129*, 154305.
- (32) Zhao, Y.-L.; Meot-Ner, M.; Gonzalez, C. Ionic Hydrogen-Bond Networks and Ion Solvation. 1. An Efficient Monte Carlo/Quantum Mechanical Method for Structural Search and Energy Computations: Ammonium/Water. *J. Phys. Chem. A* **2009**, *113*, 2967–2974.
- (33) Morrell, T. E.; Shields, G. C. Atmospheric Implications for Formation of Clusters of Ammonium and 1–10 Water Molecules. *J. Phys. Chem. A* **2010**, *114*, 4266–4271.
- (34) Delley, B. An All-Electron Numerical Method for Solving the Local Density Functional for Polyatomic Molecules. *J. Chem. Phys.* **1990**, *92*, 508–517.
- (35) Jiang, S.; Liu, Y. R.; Huang, T.; Wen, H.; Xu, K. M.; Zhao, W. X.; Zhang, W. J.; Huang, W. Study of Cl⁻(H₂O)_n (n = 1–4) Using Basin-Hopping Method Coupled with Density Functional Theory. *J. Comput. Chem.* **2014**, *35*, 159–165.
- (36) Jiang, S.; Huang, T.; Liu, Y.-R.; Xu, K.-M.; Zhang, Y.; Lv, Y.-Z.; Huang, W. Theoretical Study of Temperature Dependence and Rayleigh Scattering Properties of Chloride Hydration Clusters. *Phys. Chem. Chem. Phys.* **2014**, *16*, 19241–19249.
- (37) Brkic, B.; France, N.; Taylor, S. Oil-in-Water Monitoring Using Membrane Inlet Mass Spectrometry. *Anal. Chem.* **2011**, *83*, 6230–6236.
- (38) Xu, Y.; Nadykto, A. B.; Yu, F.; Jiang, L.; Wang, W. Formation and Properties of Hydrogen-Bonded Complexes of Common Organic Oxalic Acid with Atmospheric Nucleation Precursors. *J. Mol. Struct.: THEOCHEM* **2010**, *951*, 28–33.
- (39) Herb, J.; Nadykto, A. B.; Yu, F. Large Ternary Hydrogen-Bonded Pre-Nucleation Clusters in the Earth's Atmosphere. *Chem. Phys. Lett.* **2011**, *518*, 7–14.
- (40) Xu, W.; Zhang, R. Theoretical Investigation of Interaction of Dicarboxylic Acids with Common Aerosol Nucleation Precursors. *J. Phys. Chem. A* **2012**, *116*, 4539–4550.
- (41) Xu, W.; Zhang, R. A Theoretical Study of Hydrated Molecular Clusters of Amines and Dicarboxylic Acids. *J. Chem. Phys.* **2013**, *139*, 064312.
- (42) Contreras-García, J.; Johnson, E. R.; Keinan, S.; Chaudret, R.; Piquemal, J.-P.; Beratan, D. N.; Yang, W. NCIPLOT: A Program for Plotting Noncovalent Interaction Regions. *J. Chem. Theory Comput.* **2011**, *7*, 625–632.

- (43) Zhao, J.; Smith, J.; Eisele, F.; Chen, M.; Kuang, C.; McMurry, P. Observation of Neutral Sulfuric Acid-Amine Containing Clusters in Laboratory and Ambient Measurements. *Atmos. Chem. Phys.* **2011**, *11*, 10823–10836.
- (44) Jiang, J.; Chang, H.-C.; Lee, Y.; Lin, S. Ab Initio Studies of $\text{NH}_4^+(\text{H}_2\text{O})_{1-5}$ and the Influence of Hydrogen-Bonding Nonadditivity on Geometries and Vibrations. *J. Phys. Chem. A* **1999**, *103*, 3123–3135.
- (45) Pickard, F. C., IV; Dunn, M. E.; Shields, G. C. Comparison of Model Chemistry and Density Functional Theory Thermochemical Predictions with Experiment for Formation of Ionic Clusters of the Ammonium Cation Complexed with Water and Ammonia; Atmospheric Implications. *J. Phys. Chem. A* **2005**, *109*, 4905–4910.
- (46) Zhao, F.-Y.; Liu, C.; Gong, L.-D.; Yang, Z.-Z. Theoretical Studies on $\text{NH}_4^+(\text{H}_2\text{O})_n$ ($n = 1 \sim 9$) in Terms of Quantum Chemistry and AVEEM/MM. *Acta Chim. Sinica* **2011**, *69*, 1141–1150.
- (47) Pérez, C.; Muckle, M. T.; Zaleski, D. P.; Seifert, N. A.; Temelso, B.; Shields, G. C.; Kisiel, Z.; Pate, B. H. Structures of Cage, Prism, and Book Isomers of Water Hexamer from Broadband Rotational Spectroscopy. *Science* **2012**, *336*, 897–901.
- (48) Xantheas, S. S. Cooperativity and Hydrogen Bonding Network in Water Clusters. *Chem. Phys.* **2000**, *258*, 225–231.
- (49) Liu, Y.-R.; Wen, H.; Huang, T.; Lin, X.-X.; Gai, Y.-B.; Hu, C.-J.; Zhang, W.-J.; Huang, W. Structural Exploration of Water, Nitrate/Water, and Oxalate/Water Clusters with Basin-Hopping Method Using a Compressed Sampling Technique. *J. Phys. Chem. A* **2014**, *118*, 508–516.
- (50) Klots, C. E. Systematics of Evaporation. *Z. Phys. D-Atoms, Molecules and Clusters* **1991**, *20*, 105–109.
- (51) Huang, W.; Bulusu, S.; Pal, R.; Zeng, X. C.; Wang, L.-S. Structural Transition of Gold Nanoclusters: From the Golden Cage to the Golden Pyramid. *ACS Nano* **2009**, *3*, 1225–1230.
- (52) Wu, Z.; Jin, R. Stability of the Two Au-S Binding Modes in $\text{Au}_{25}(\text{SG})_{18}$ Nanoclusters Probed by NMR and Optical Spectroscopy. *ACS Nano* **2009**, *3*, 2036–2042.
- (53) Wang, L.-M.; Pal, R.; Huang, W.; Zeng, X. C.; Wang, L.-S. Observation of Earlier Two-to-Three Dimensional Structural Transition in Gold Cluster Anions by Isoelectronic Substitution: MAu_n^- ($n = 8 \sim 11$; M= Ag, Cu). *J. Chem. Phys.* **2010**, *132*, 114306.
- (54) Xu, K.-M.; Huang, T.; Wen, H.; Liu, Y.-R.; Gai, Y.-B.; Zhang, W.-J.; Huang, W. A Density Functional Study of Phosphorus-Doped Gold Clusters: Au_nP^- ($n = 1 \sim 8$). *RSC Adv.* **2013**, *3*, 24492–24502.
- (55) Do, H.; Besley, N. A. Structural Optimization of Molecular Clusters with Density Functional Theory Combined with Basin Hopping. *J. Chem. Phys.* **2012**, *137*, 134106.
- (56) Saykally, R. J.; Wales, D. J. Pinning Down the Water Hexamer. *Science* **2012**, *336*, 814–815.
- (57) Swope, W. C.; Andersen, H. C.; Berens, P. H.; Wilson, K. R. A Computer Simulation Method for the Calculation of Equilibrium Constants for the Formation of Physical Clusters of Molecules: Application to Small Water Clusters. *J. Chem. Phys.* **1982**, *76*, 637.
- (58) Galashev, A. A Computer Study of Ammonium Adsorption on Water Clusters. *Russ. J. Phys. Chem. B* **2013**, *7*, 502–508.
- (59) Zhu, Y.-P.; Liu, Y.-R.; Huang, T.; Jiang, S.; Xu, K.-M.; Wen, H.; Zhang, W.-J.; Huang, W. Theoretical Study of the Hydration of Atmospheric Nucleation Precursors with Acetic Acid. *J. Phys. Chem. A* **2014**, *118*, 7959–7974.
- (60) Temelso, B.; Morrell, T. E.; Shields, R. M.; Allodi, M. A.; Wood, E. K.; Kirschner, K. N.; Castonguay, T. C.; Archer, K. A.; Shields, G. C. Quantum Mechanical Study of Sulfuric Acid Hydration: Atmospheric Implications. *J. Phys. Chem. A* **2012**, *116*, 2209–2224.
- (61) Loukonen, V.; Kurtén, T.; Ortega, I.; Vehkamäki, H.; Padua, A.; Sellegrí, K.; Kulmala, M. Enhancing Effect of Dimethylamine in Sulfuric Acid Nucleation in the Presence of Water – A Computational Study. *Atmos. Chem. Phys.* **2010**, *10*, 4961–4974.
- (62) Weber, K. H.; Morales, F. J.; Tao, F.-M. Theoretical Study on the Structure and Stabilities of Molecular Clusters of Oxalic Acid with Water. *J. Phys. Chem. A* **2012**, *116*, 11601–11617.
- (63) Weber, K. H.; Liu, Q.; Tao, F.-M. Theoretical Study on Stable Small Clusters of Oxalic Acid with Ammonia and Water. *J. Phys. Chem. A* **2014**, *118*, 1451–1468.
- (64) Seinfeld, J. H.; Pandis, S. N. *Atmospheric Chemistry and Physics: From Air Pollution to Climate Change*, 2nd ed.; John Wiley & Sons, Inc.: New York, 2006.
- (65) Cohen, A. J.; Mori-Sánchez, P.; Yang, W. Insights into Current Limitations of Density Functional Theory. *Science* **2008**, *321*, 792–794.
- (66) Johnson, E. R.; Keinan, S.; Mori-Sánchez, P.; Contreras-García, J.; Cohen, A. J.; Yang, W. Revealing Noncovalent Interactions. *J. Am. Chem. Soc.* **2010**, *132*, 6498–6506.